RSC Advances

PAPER

View Article Online
View Journal | View Issue

Cite this: *RSC Adv.*, 2018, **8**, 33243

Identification of the dominant hydrogeochemical processes and characterization of potential contaminants in groundwater in Qingyuan, China, by multivariate statistical analysis†

Zuobing Liang, Jianyao Chen,* Tao Jiang, Kun Li, Lei Gao, Zhuowei Wang, Shaoheng Li and Zhenglan Xie

In karst areas, groundwater is an important water source for drinking and irrigation purposes; however, karst aquifers are vulnerable and recovery from damage is difficult. We collected surface water (pond and river water) and groundwater (hand-pump well, dug well, and borehole water) samples in Qingyuan city, China, to determine the major chemicals in the water with the primary goals of evaluating the geochemical composition, identifying the geochemical processes governing the water chemistry, and identifying the probable sources of potential contaminants in shallow and deep groundwater in the study area. The results revealed marked differences in water chemistry between shallow and deep groundwater. The groundwater composition was largely controlled by rock–water interactions, particularly the dissolution of evaporite minerals (*e.g.*, calcite, gypsum, and anhydrite), and ion exchange processes were important drivers of the chemical compositions of groundwater in the study area. Moreover, in shallow and deep groundwater, Mg^{2+} and SO_4^{2-} concentrations were increased due to the long residence time of deep groundwater, while K^+ and Na^+ concentrations were decreased due to anthropogenic input. Finally, factor analysis of the major and trace elements differentiated between anthropogenic and geogenic sources of potential contaminants in karst aquifers.

Received 16th July 2018
Accepted 16th September 2018

DOI: 10.1039/c8ra06051g

rsc.li/rsc-advances

1. Introduction

Over the last few decades, rapid growth of urban population has resulted in dramatic increases in water use and wastewater production in many developing countries worldwide.[1] Because groundwater is a major water resource, anthropogenic degradation of groundwater quality has attracted significant interest. In particular, groundwater from karst aquifers is an important drinking water resource in karst regions, but is particularly vulnerable to anthropogenic contamination due to the porous nature of karst terrain.[2,3] Groundwater hydrochemistry and quality evaluations are used to clarify mineralization processes, and are also useful for exploring water–rock interactions and analyzing area-specific environmental issues.[4]

Groundwater studies largely focus on the main hydrochemical processes that affect groundwater quality and hydrochemical profiles.[5,6] Hydrochemical analyses can help define chemical reactions produced by water–rock interactions, and water–rock interactions or anthropogenic sources of pollution can also be interpreted in the context of related reactions and processes.[7,8]

Qingyuan city is located in a typical karst area in Guangdong Province, China, characterized by high spatial hydrogeological heterogeneities. This karst environment is vulnerable and recovery of function of karst aquifers is difficult once damaged. Issues related to pollution-intense industry relocation driven by globalization, at both a national and regional scale, are becoming increasingly relevant under current policy-making and environmental regulations. Guangdong Province is considered a pollution haven for overseas industries, and Qingyuan, located in northern Guangdong Province, is becoming a pollution haven for the Pearl River Delta.[9] Qingyuan is the largest prefecture-level city in Guangdong Province, and anthropogenic sources of pollution therein are mainly derived from extensive urbanization, farming and agriculture practices, and industrial activities. Evaluating the groundwater quality and impact of human activities in this large karst area is a necessary and pressing task. Therefore, the objectives of this study were to (1) examine seasonal variations in water chemistry, (2) determine the geochemical processes and factors controlling the chemical compositions of karst water, (3) elucidate the chemical evolution of surface water and groundwater, and (4) identify probable sources of potential contaminants.

Guangdong Provincial Key Laboratory of Urbanization and Geo-simulation, School of Geography and Planning, Sun Yat-Sen University, Guangzhou, PR China. E-mail: chenjyao@mail.sysu.edu.cn; Tel: +86 20 84115930

† Electronic supplementary information (ESI) available. See DOI: 10.1039/c8ra06051g

2. Study area

The study area was in Qingyuan (23°26′–25°11′N, 111°55′–113°55′E), northern Guangdong Province, China, and covered about 1.9 × 10^4 km^2 (Fig. 1). There are three morphologically distinct formations in the study area: plains, hills, and mountains. The maximum elevation, in the mountainous region, is nearly 1570 m and the minimum elevation, in the plains, is approximately 4 m. The area has a subtropical monsoon climate with an annual mean temperature of 20.6 °C and annual precipitation of 1556 mm. Several rivers run through the plain, including Lianjiang River, Pajiang River, Beijiang River, and their tributaries.

Two types of rocks are exposed in the study area: limestone formed from the Late Paleozoic to Mesozoic (Triassic) and granite formed during the Yanshanian. Carboniferous carbonate rocks are widely exposed and typical synclinal–tectonic karst basins associated with peak-forest plains and peak-cluster depressions are widely distributed. Fissures and fractures have extensively developed in carbonate rocks, promoting karstification of the basin, and the high precipitation ensures abundant groundwater resources.

2.1 Sample collection and pretreatment in the field

The water samples were collected from three ponds, 13 hand-pump wells, 11 dug wells, 19 boreholes, and nine other locations along various rivers. The sampling locations are shown in Fig. 1. To investigate seasonal variability, samples were collected at the three ponds and 13 of the boreholes on select days during both the dry season (January 2017) and rainy season (September 2017).

Before sample collection, each sample bottle was washed with nitric acid to remove cations and then rinsed with distilled water. In addition, the sample bottles were rinsed thrice with the same water before sample collection.

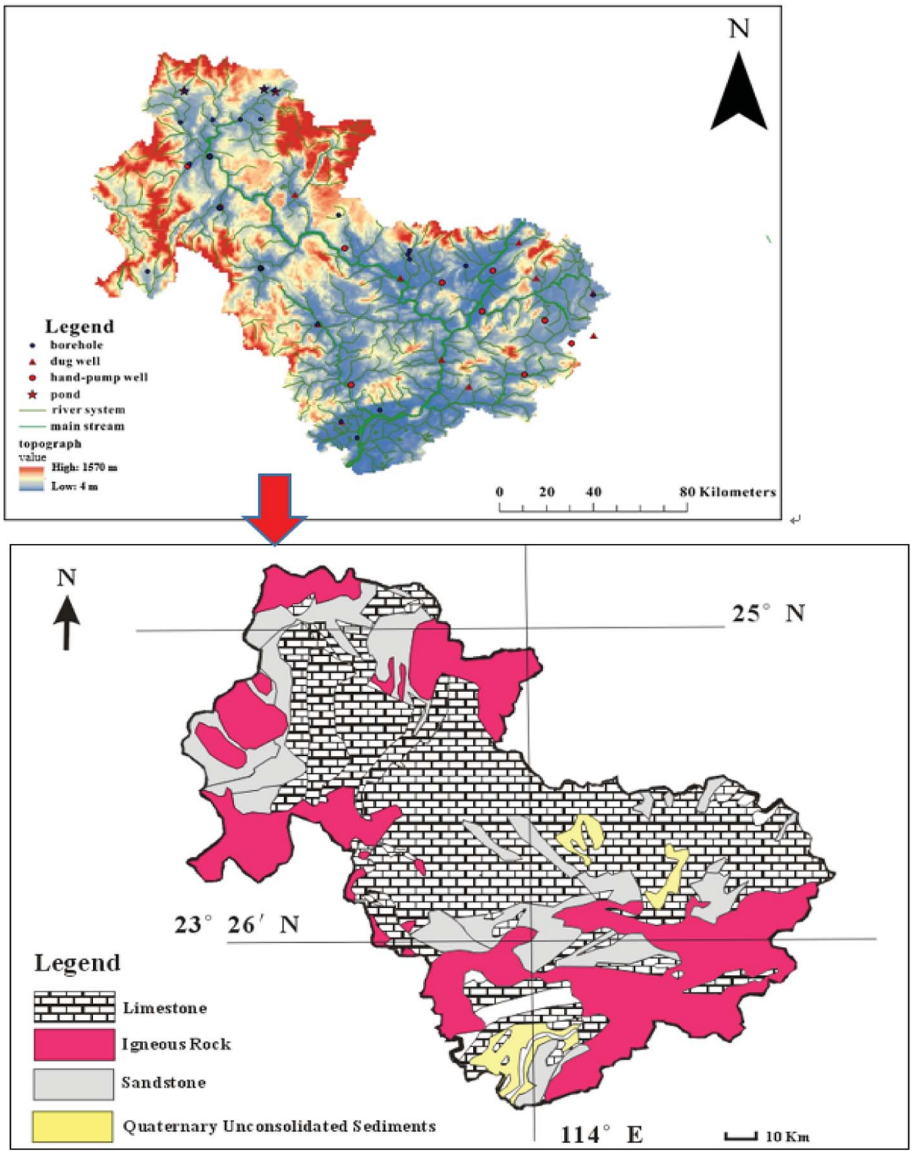

Fig. 1 Sampling sites of the study area.

2.2 Analytical methods

Environmental parameters (pH, electrical conductivity (EC), and temperature) were stabilized and measured with a multi-parameter measurement device (DR/800; HACH, Loveland, CO, USA) during pumping. Water samples were filtered through 0.22 μm pore-size membrane filters (Millipore, Burlington, MA, USA) to remove suspended particles and microorganisms, after which major cation samples were acidified to pH < 2 with HCl immediately after sampling. All major ions (Cl^-, NO_3^-, PO_4^{3-}, and SO_4^{2-}) except HCO_3^- were analyzed using a DX-600 ion chromatograph (Dionex, Sunnyvale, CA, USA) in the laboratory of the School of Environmental Science and Engineering, Sun Yat-sen University (Guangzhou, China), with a detection limit of 0.1 ppm. HCO_3^- was titrated immediately in the field using a portable testing kit (Merck KGaA Co., Darmstadt, Germany), with an accuracy of 0.05 mmol L^{-1}. The major cations were detected with inductively coupled plasma optical emission spectrometry (Optima 8300; Perkin-Elmer, Waltham, MA, USA) with a detection limit of 0.05 ppm for Ca^{2+}, Mg^{2+}, K^+, and Na^+, and 0.01 ppm for Ba, Sr, Fe, Cr, Mn, Co, Ni, Cu, Zn, As, Se, Mo, Cd, and Pb at the laboratory of the Instrumental Analysis & Research Center, Sun Yat-sen University. The analytical precision of the major ions was within 1%. The ion balance errors of most water samples were <10%, and some were >10 (Appendix A). The ion balance error higher than 10% in some samples may result from the existence of unanalyzed anions and cations such as organic acids in water.[10,11] Still, there should be further research on the factors affecting the higher error of ion balance.

3. Results and discussion

3.1 Field parameters

Table 1 presents the major physiochemical and chemical properties of the water samples, which were analyzed on select days in both the dry (January 2017) and rainy (September 2017) seasons. The average temperature varied seasonally in pond water and was 17.3 ± 2.35 °C and 20.1 ± 7.65 °C in the dry and rainy seasons, respectively. Meanwhile, the average temperature of the river samples in the rainy season was 29.5 ± 2.25 °C. During the dry season, the average temperatures of the hand-pump and dug well water were 20.1 ± 2.66 °C and 22.8 ± 1.93 °C, respectively. The average temperatures of deep groundwater (*i.e.*, boreholes) in the dry and rainy seasons were 19.9 ± 2.53 °C and 25.5 ± 1.92 °C, respectively, indicative of seasonal variation according to surface air temperature in the karst area.

The average EC values varied substantially among water samples but which did not show a variation characteristic in the vertical spatial distribution. However, the average EC values for ponds and boreholes were lower in the dry season than the rainy season. Meanwhile, the pH of pond water was 5.46–7.13 in the dry season and 6.94–8.23 in the rainy season. The minimum value of pond water was sampled in a small pond underlaid by sandy stone that provided drinking water for nearby residents and was mainly recharged by rain water. According to Huang *et al.*,[12] the pH values in a coastal mega-city in South China was 4.56 over a 5 years period. The short water–rock reaction time in the small pond and low EC values of rain water may have been responsible for the lower pH and EC values.

The dissolved oxygen (DO) concentration of the surface (*i.e.*, pond and river) waters varied from 1.84 mg L^{-1} to 7.44 mg L^{-1}, whereas those of shallow groundwater (*i.e.*, hand-pump well and dug well water) ranged widely from 3.11 mg L^{-1} to 7.48 mg L^{-1} (average: 5.00 mg L^{-1}). Meanwhile, the DO concentration of deep groundwater was 1.71–3.80 mg L^{-1} (average: 2.81 mg L^{-1}) in the dry season and 1.13–6.51 mg L^{-1} (average: 2.22 mg L^{-1}) in the rainy season.

3.2 Water chemistry

Piper trilinear diagrams summarize the differences in hydrochemical composition among water sources.[13] Fig. 2 presents the piper trilinear equivalence diagrams of the samples. Overall, the hydrochemistry was dominated by alkaline earth metal ions, although weak acids, Ca^{2+}, and bicarbonate also made substantial contributions to the water chemistry composition. Overall, according to the analysis of major ionic composition, Ca–HCO_3 and Ca–SO_4 were the two main waters types, although three of the pond samples had Ca–HCO_3-type water. The majority of hand-pump and dug well samples had Ca–HCO_3-type water, probably as a consequence of calcite dissolution. Most borehole and river samples were Ca–HCO_3 type, accompanied by Ca–SO_4 in several boreholes and river samples. Ca^{2+} and HCO_3^- ions result not only from dissolution of carbonate rocks, but potentially also from the hydrolysis of sandstone cement or, to a limited degree, feldspar dissolution in basement rocks.[14,15]

Most river samples and some hand-pump and dug well samples tended to be slightly enriched in SO_4^{2-} and Cl^-. The Cl^- concentrations in the dug well water reached 1.82 meq L^{-1}, and the maximum SO_4^{2-} concentrations in the river, hand-pump well, and dug well samples were 1.21 meq L^{-1}, respectively (Table 1). Na^+ and K^+ concentrations in shallow groundwater also tended to be enriched compared to the deep groundwater samples. In addition to natural sources, anthropogenic activities (*e.g.*, deicing, fertilizer, and wastewater) produce K^+ and Na^+ ions that can enter the groundwater,[14,16] and almost all shallow groundwater samples from both the residential and karst areas were more vulnerable to contamination. By contrast, the deep groundwater tended to be more enriched in Mg^{2+} than the shallow groundwater. According to the incongruent dissolution of dolomite, the increase in Mg^{2+} corresponded to the increased residence time in limestone.[17] Since the deep groundwater was in the karst area, the enrichment in Mg^{2+} may have resulted from the long residence time of groundwater.

3.3 Chemical evolution of groundwater

The soluble ions in natural waters mainly originated from rock and soil weathering and anthropogenic inputs, and partly from atmospheric inputs. The influence of rock weathering, evaporation, and precipitation on water chemistry was evaluated with Gibbs' diagrams. Fig. 3a and b show Gibbs' plots of total dissolved solids according to the ion ratios $Na^+/(Na^+ + Ca^{2+})$ and

Table 1 Major chemical composition of surface water and groundwater samples

	Sample		EC (μs cm^{-1})	pH	DO (mg L^{-1})	Temp. (°C)	HCO_3^-	Cl^-	NO_3^-	SO_4^{2-}	K^+	Na^+	Ca^{2+}	Mg^{2+}	TDS (mg L^{-1})
							meq L^{-1}								
Ponds	Rainy season ($n = 3$)	Min	12.2	6.94	3.22	23.8	0.50	0.03	0.01	0.22	0.01	0.02	0.05	0.01	34.2
		Mean	281	7.51	3.61	26.6	2.53	0.35	0.36	0.35	0.13	0.42	2.25	0.46	245
		Max	572	8.23	1.84	31	4.00	0.92	1.04	0.38	0.35	0.76	4.74	0.21	437
		SD	280	3.63	1.99	7.65	1.82	0.49	0.59	0.12	0.19	0.38	2.35	0.62	202
	Dry season ($n = 3$)	Min	12.1	5.46	3.62	14.6	0.10	0.01	0.00	0.01	0.00	0.00	0.07	0.05	9.28
		Mean	444	6.60	4.97	17.3	3.57	0.36	0.10	0.25	0.13	0.22	2.61	0.64	313
		Max	721	7.13	7.44	18.4	5.84	0.99	0.25	0.40	0.35	0.43	4.55	1.62	470
		SD	379	0.99	2.14	2.35	3.05	0.55	0.13	0.21	0.19	0.21	2.30	0.85	263
Rivers	Rainy season ($n = 9$)	Min	35.7	6.70	2.50	26.8	0.00	0.04	0.04	0.10	0.01	0.03	0.98	0.21	104
		Mean	213	7.75	5.65	29.5	1.15	0.12	0.14	0.48	0.05	0.13	3.30	0.56	208
		Max	339	8.12	7.13	31.5	3.00	0.27	0.54	1.21	0.10	0.33	6.35	1.18	344
		SD	111	0.62	1.87	2.25	1.25	0.07	0.15	0.35	0.03	0.09	1.80	0.35	86.6
Hand pump wells	Dry season ($n = 13$)	Min	167	5.81	3.24	13.5	0.59	0.12	0.00	0.14	0.01	0.02	0.67	0.10	105
		Mean	448	6.82	4.61	20.1	2.95	0.45	0.09	0.62	0.17	0.23	3.32	0.44	310
		Max	675	7.43	6.16	22.3	5.20	1.05	0.22	1.21	0.48	0.49	5.30	1.21	503
		SD	144	0.46	0.90	2.66	1.21	0.30	0.07	0.34	0.14	0.17	1.32	0.31	109
Dug wells	Dry season ($n = 11$)	Min	72.9	5.70	3.11	16.2	0.44	0.05	0.00	0.08	0.00	0.00	0.39	0.07	46
		Mean	362	6.65	4.98	20.1	2.16	0.55	0.10	0.46	0.20	0.30	2.31	0.40	240
		Max	942	7.56	7.48	22.8	5.35	1.82	0.30	1.21	0.87	0.91	6.05	1.37	620
		SD	254	0.60	2.31	1.93	1.78	0.58	0.10	0.39	0.26	0.31	1.68	0.41	173
Boreholes	Rainy season ($n = 19$)	Min	32	6.08	1.13	22.6	1.10	0.03	0.02	0.01	0.02	0.03	0.30	0.08	131
		Mean	377	7.33	2.22	25.5	3.61	0.17	0.08	2.51	0.10	0.47	2.98	0.96	432
		Max	1735	8.41	6.51	30.0	7.20	0.48	0.28	42.0	0.60	3.51	17.0	5.68	2653
		SD	353	0.56	1.27	1.92	1.66	0.14	0.08	9.56	0.14	0.83	3.61	1.28	550
	Dry season ($n = 13$)	Min	201	6.40	1.71	14.2	1.08	0.02	0.00	0.01	0.01	0.01	0.75	0.11	134
		Mean	473	7.40	2.81	19.9	3.24	0.37	0.02	1.98	0.09	0.21	2.52	1.25	381
		Max	1494	8.49	3.80	22.4	10.61	1.69	0.21	15.78	0.26	0.90	8.80	6.03	1301
		SD	375	0.60	0.65	2.15	2.53	0.45	0.06	4.55	0.07	0.27	2.30	1.53	334

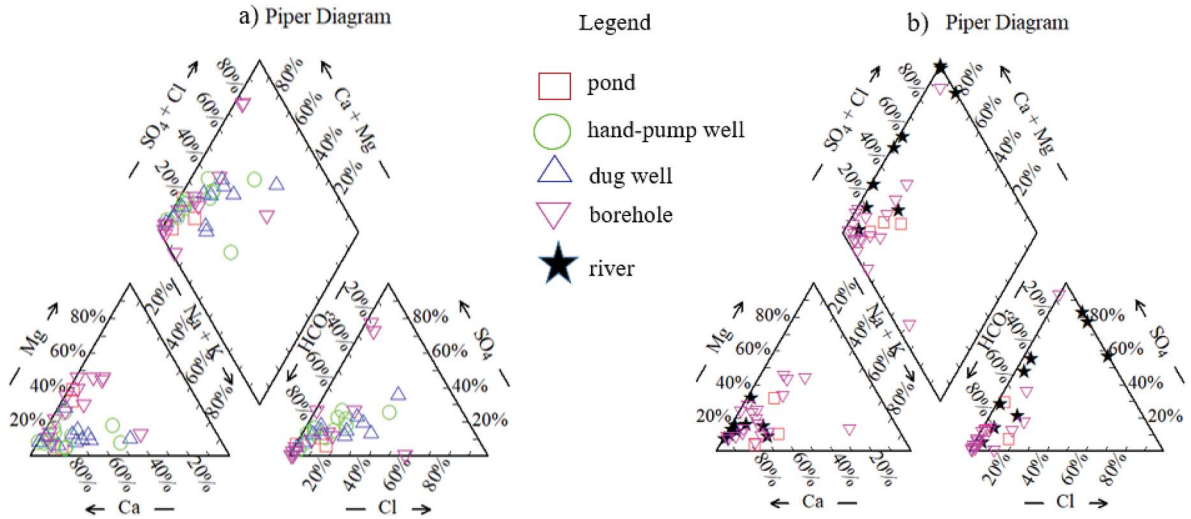

Fig. 2 Piper diagram for hydro-chemical types of the analyzed water samples ((a): dry season, (b): rainy season).

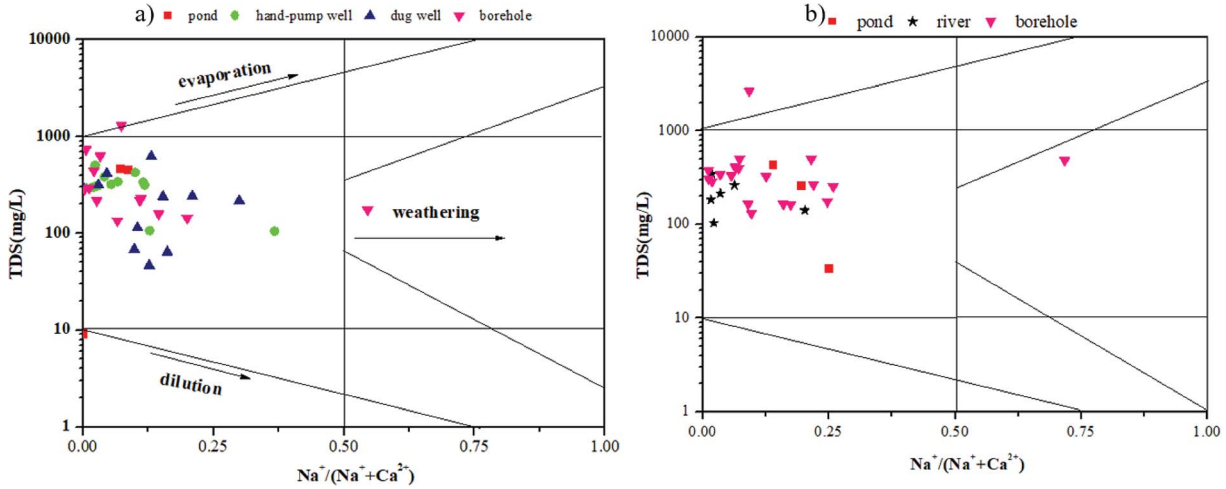

Fig. 3 Ratios of Na^+ to (Na^+ + Ca^{2+}) as a function of TDS for all samples (a: dry season, b: rainy season).

$Cl^-/(Cl^- + HCO_3^-)$ of groundwater in the two seasons. Most data points were distributed in areas of end members of the dominant rocks, confirming that the groundwater chemistry in the study area was dominated by the interaction between water and aquifer materials. In addition, one pond sample in the study area was dominated by atmospheric precipitation.

The chemical properties of the groundwater in the study area were mainly controlled by natural geochemical processes, although anthropogenic activities also influenced the chemical properties of groundwater, especially in the shallow part of the aquifer. In aquifer systems, the chemical evolution of groundwater results from interactions among various processes, which are difficult to identify based on the solute balance.[14] However, the origins of ions and processes that control their concentrations can be determined by plotting bivariate diagrams.[18] Therefore, we created several plots of the relationships among major elements to identify the origin and processes contributing to groundwater mineralization.

The Na^+/Cl^- ratio is considered to be one of the most important indicators of the origin of groundwater, where a ratio of 1 represents halite dissolution.[19] The plot of Na^+ *versus* Cl^- revealed a trend from excess Cl^- ($Cl^- > Na^+$) toward the 1 : 1 stoichiometric ratio line for hand-pump well, dug well, and borehole water samples in the dry season (Fig. 4a). Meanwhile, most points for river water were situated along the halite dissolution line, although several high Na^+/Cl^- ratios were observed in borehole water samples in the rainy season (Fig. 4b). The excess Na^+ over Cl^- ions may have resulted from three processes:[20] (1) cation exchange reactions; (2) weathering of feldspars in sandstone samples, and (3) reaction of silicate minerals derived mainly from sandstone weathering. Conversely, the depletion of Na^+ concentrations relative to Cl^- concentrations in the upper aquifer may have resulted from the reaction of silicate minerals, or a second type of ionic exchange in which Na^+ was removed from the complex and replaced by Ca^{2+}. Hence, during the dry season, the abnormal samples in the borehole waters above the

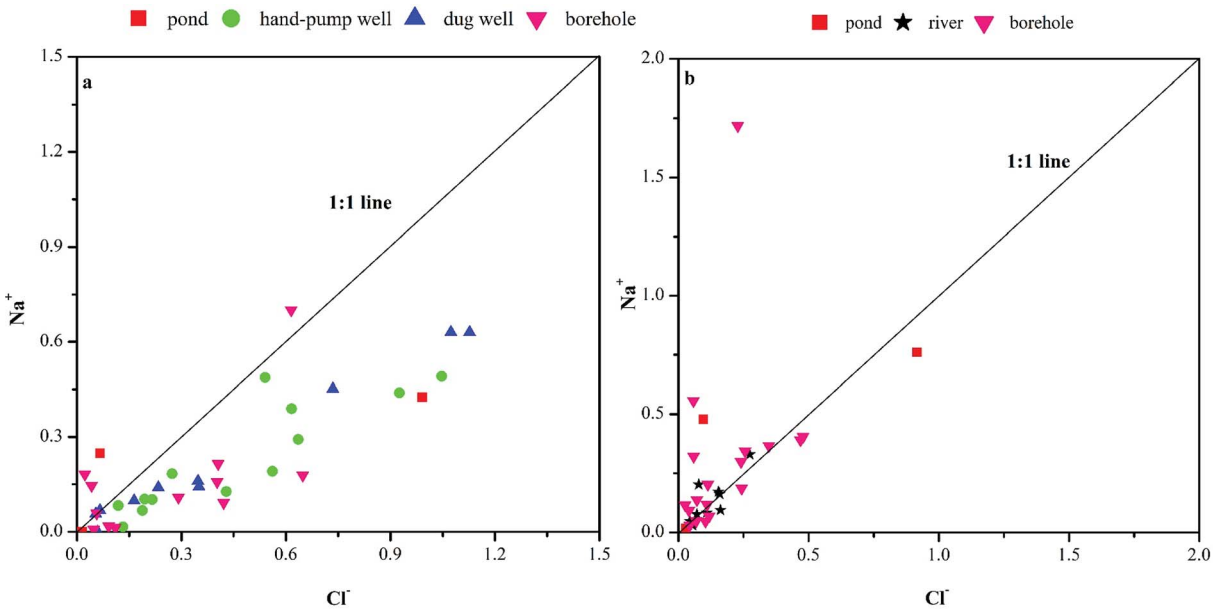

Fig. 4 The plots of Na^+ *versus* Cl^- (meq L^{-1}).

1 : 1 line indicated that halite dissolution was not the only source of Na^+. Samples with Na^+/Cl^- ratios lower than 1 accounted for 92% and 64% of shallow and deep groundwater samples, respectively, further indicative of additional Na^+ sources. However, in the rainy season, the excess of Na^+ relative to Cl^- concentrations in most borehole samples might have reflected cation exchange reactions or mineral dissolution in deep groundwater. Overall, precipitation appeared to greatly influence the deep groundwater chemistry in the karst area.

In most samples, HCO_3^- was the dominant anion, accounting for approximately 60–80% of the total dissolved anions. The HCO_3^- concentrations were 0.10–4.76 meq L^{-1} for pond water, 0.44–5.35 meq L^{-1} for shallow groundwater and 1.08–10.61 meq L^{-1} for deep groundwater during the dry season (Table 1). During the rainy season, the HCO_3^- concentrations were 0.00–3.00 meq L^{-1} for river water and 1.10–7.20 meq L^{-1} for deep groundwater. In the plot of HCO_3^- *versus* Ca^{2+}, most hand-pump well water points were above the 1 : 1 stoichiometric ratio line, dug well water points were clustered around the 1 : 1 stoichiometric ratio line, and borehole water points were below the 1 : 1 stoichiometric line (Fig. 5a and b). Meanwhile, in the $Ca^{2+} + Mg^{2+}$ *versus* HCO_3^- plot (Fig. 6a and b), the dug well, river, and hand-pump well waters mostly had $(Ca^{2+} + Mg^{2+})/HCO_3^-$ ratios above 1 : 1, indicating that additional sources besides carbonated weathering accounted for the excess Mg^{2+} and Ca^{2+} relative to HCO_3^-.

Related studies reported that excess $Ca^{2+} + Mg^{2+}$ with respect to HCO_3^- in karst aquifers may result from calcite dissolution,

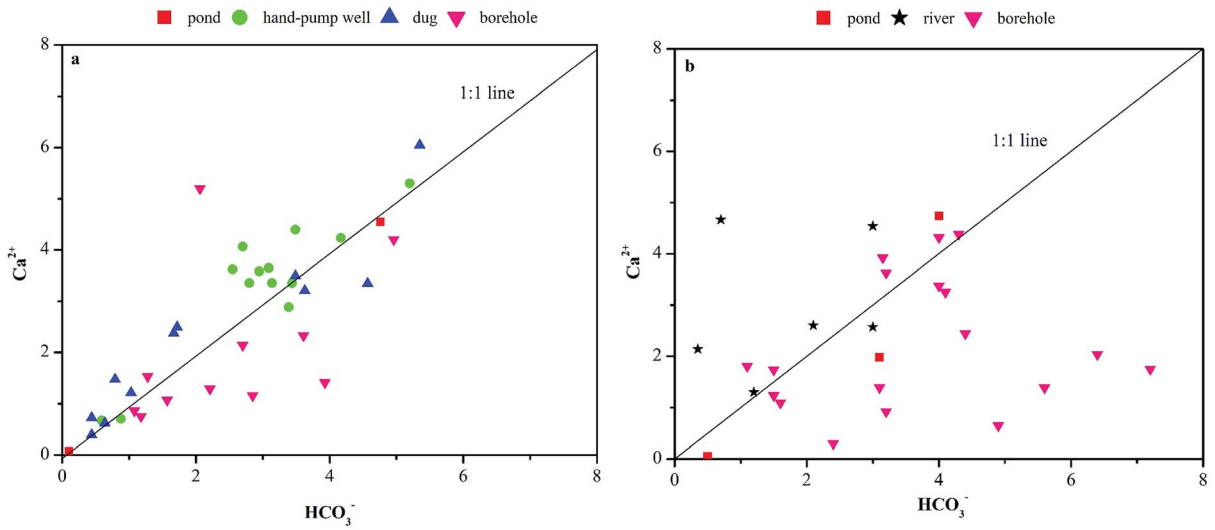

Fig. 5 Plots of Ca^{2+} *versus* HCO_3^- (meq L^{-1}).

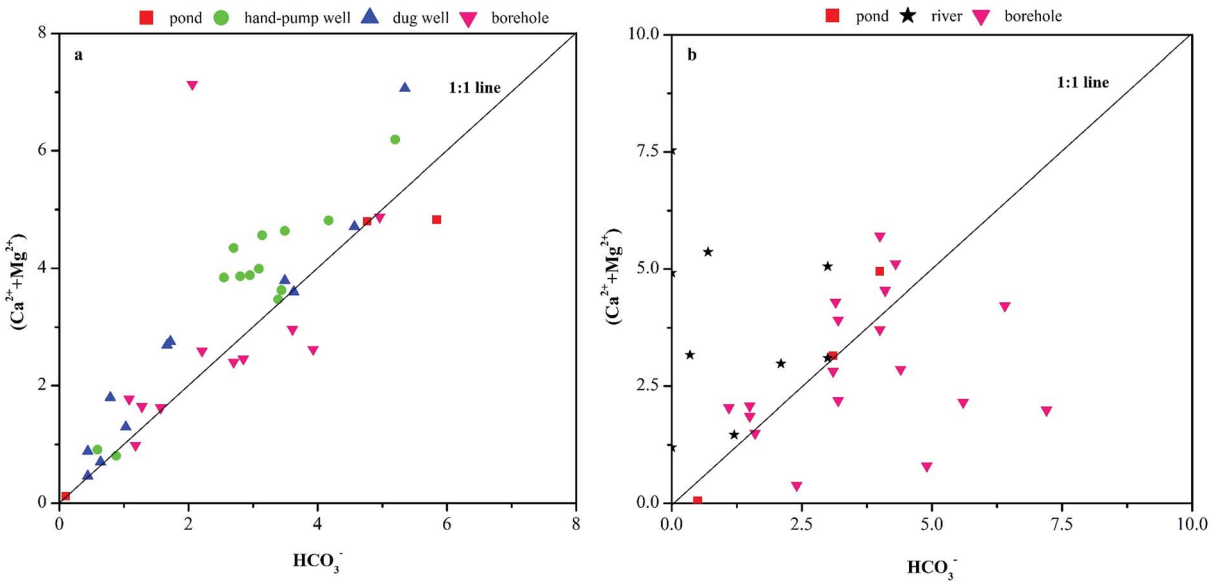

Fig. 6 Plots of (Ca^{2+} + Mg^{2+}) *versus* HCO_3^- (meq L^{-1}).

and the majority of Ca^{2+}, Mg^{2+}, and HCO_3^- ions from shallow groundwater may have largely originated from carbonate dissolution. Meanwhile, the plot of Ca^{2+} + Mg^{2+} *versus* HCO_3^- during the dry season (Fig. 6a) showed that most borehole water points were clustered along the dolomite line, indicating that the Mg^{2+}, Ca^{2+}, and HCO_3^- in this aquifer shared the same origin; however, an excess of HCO_3^- over Ca^{2+} + Mg^{2+} was observed during the rainy season (Fig. 6b). Thus, rock type was not the only factor influencing the Ca^{2+}, Mg^{2+} and HCO_3^- ions in the borehole waters among different seasons.

In the studied aquifer system, carbonate dissolution is the dominant process contributing to groundwater solutes (Ca^{2+}, Mg^{2+}, and HCO_3^-). The mean Mg^{2+}/Ca^{2+} ratios of the hand-pump well, dug well, and borehole water samples were 0.15, 0.17, and 0.55, respectively. The Mg^{2+}/Ca^{2+} ratio sometimes approached a value of 0.33, indicating the influence of calcite dissolution.[14] According to Appendix B, the lithology in deep groundwater (borehole) is mainly controlled by limestone, but the lithology in shallow groundwater (hand-pump well and dug well) all belongs to unconsolidated sediments. Therefore, lithology may not the main factor affecting Mg^{2+}/Ca^{2+} ratio in groundwater. As we can see from Fig. 7a and b, Mg^{2+}/Ca^{2+} ratios in deep groundwater were higher than shallow groundwater in general, well depth in hand-pump well and dug well are all below 8 m, and all above 60 m in borehole (Appendix B). It main conclude that higher Mg^{2+}/Ca^{2+} ratio in deep groundwater was likely resulted from the longer residence time of groundwater. During the rainy season, the karst aquifer was mainly recharged

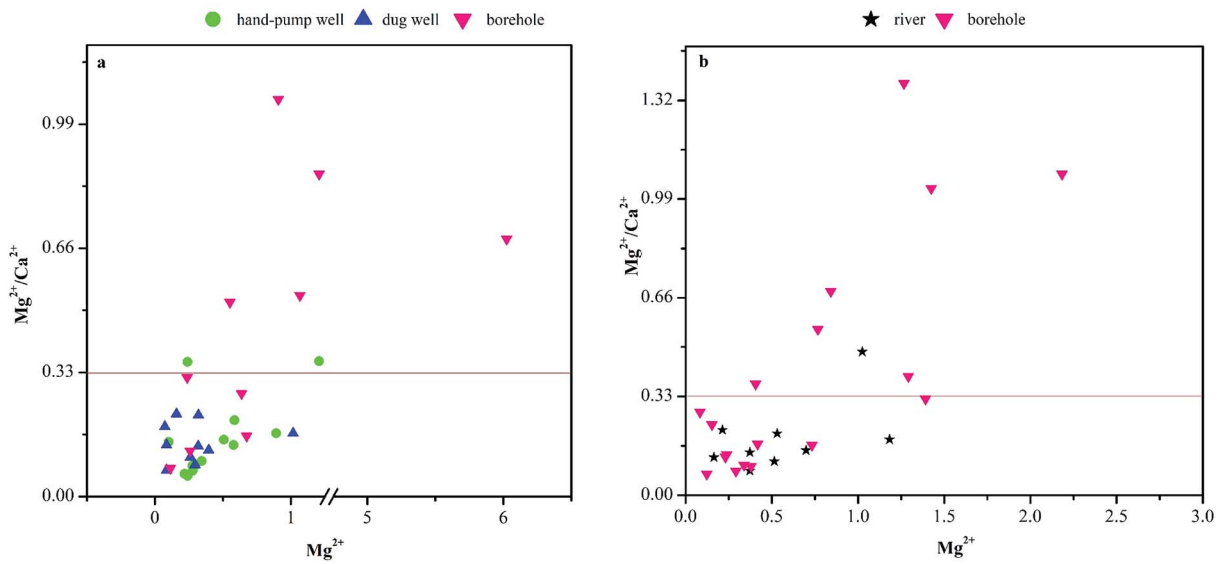

Fig. 7 Plots of Mg^{2+}/Ca^{2+} *versus* Mg^{2+} (meq L^{-1}).

by precipitation, resulting in a short groundwater residence time based on the heterogeneity of karst aquifers and depleted Mg^{2+} compared with the deep groundwater in the dry season. Hence, the groundwater residence time within carbonate aquifers may explain the difference in Mg^{2+} proportions among different aquifers.

The plots of $(Ca^{2+} + Mg^{2+})$ *versus* $(HCO_3^- + SO_4^{2-})$ (Fig. 8a and b) and Ca^{2+} *versus* SO_4^{2-} (Fig. 8c and d) were used to identify the sources of Ca^{2+}, Mg^{2+}, and SO_4^{2-}. Most groundwater samples, except the hand-pump well water samples, showed a trend toward excess Ca^{2+} ($Ca^{2+} > SO_4^{2-}$) above the 2 : 1 line in the Ca^{2+} *versus* SO_4^{2-} plot, and a strong, significant linear relationship following a 1 : 1 ratio in the $(Ca^{2+} + Mg^{2+})$ *versus* $(HCO_3^- + SO_4^{2-})$ plot (Fig. 8a and b). This indicated that Ca^{2+}, Mg^{2+}, SO_4^{2+}, and HCO_3^- were derived from the dissolution of calcite, dolomite, and gypsum.[21] In addition, the Ca^{2+} *versus* SO_4^{2-} plots of the river and borehole water samples showed a trend toward excess Ca^{2+} ($Ca^{2+} > SO_4^{2-}$) above the 2 : 1 line during the rainy season. Meanwhile, good correlations between Ca^{2+} and SO_4^{2-} were observed among the hand-pump well, dug well, and borehole water samples (Fig. 8a), suggesting that the increased SO_4^{2-} concentrations were driven by gypsum and anhydrite dissolution.[22]

The studied aquifer system is composed of silicate minerals; therefore, the dissolution resulting from silicate weathering may have contributed to the groundwater chemistry. The bivariate mixing diagrams of Na^+-normalized Mg^{2+} *versus* Na^+-normalized Ca^{2+} (Fig. 9a and b) could be used to evaluate the influence of silicate weathering.[14] The observed waters were marked by carbonate dissolution, but one of the pond water samples was close to the global average silicate domain, indicating that carbonate dissolution was prominent, although silicate weathering also influenced the groundwater solutes (Fig. 9a and b).

Ca^{2+} and Mg^{2+} can be produced from silicate and carbonate weathering.[23] Calcite and anorthite produce similar molar concentrations of Ca^{2+} and HCO_3^-, but no SiO_2. Meanwhile, the incongruent dissolution of feldspars, micas, and pyroxenes, as well as anthropogenic activities (*e.g.*, deicing, fertilizer, and wastewater) produce K^+ and Na^+, which enter the groundwater. Moreover, HCO_3^- in groundwater can originate from carbonate dissolution, silicate weathering, oxidation of organic matter or biogenic CO_2 dissolution.

In this study, most water of the samples were depleted in Na^+ relative to Cl^-. The excess of Cl^- relative to Na^+ was suggestive of silicate mineral reactions[24] or other forms of ionic

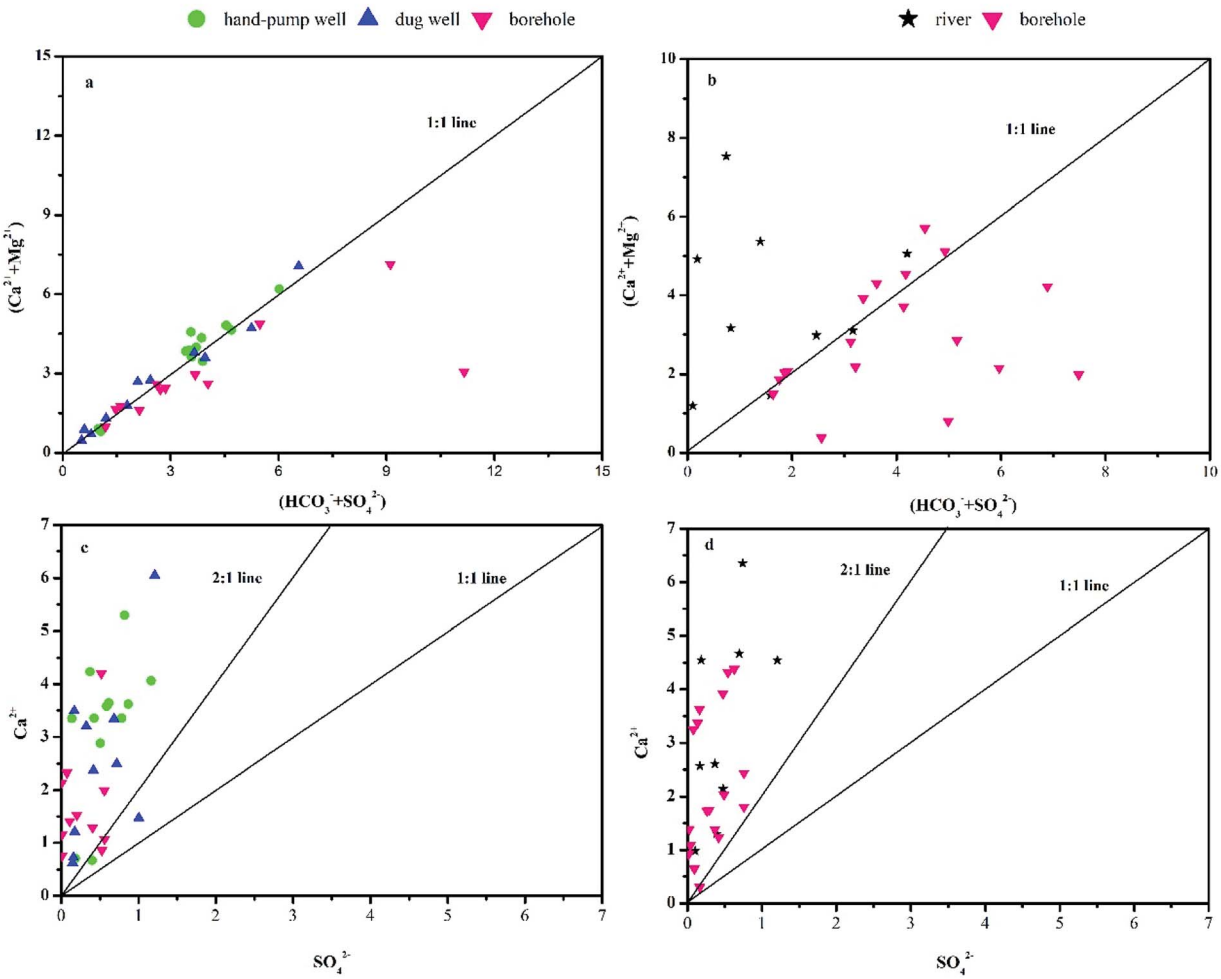

Fig. 8 Plots of $(Ca^{2+} + Mg^{2+})$ *versus* $(HCO_3^- + SO_4^{2-})$ and Ca^{2+} *versus* SO_4^{2-} (meq L^{-1}).

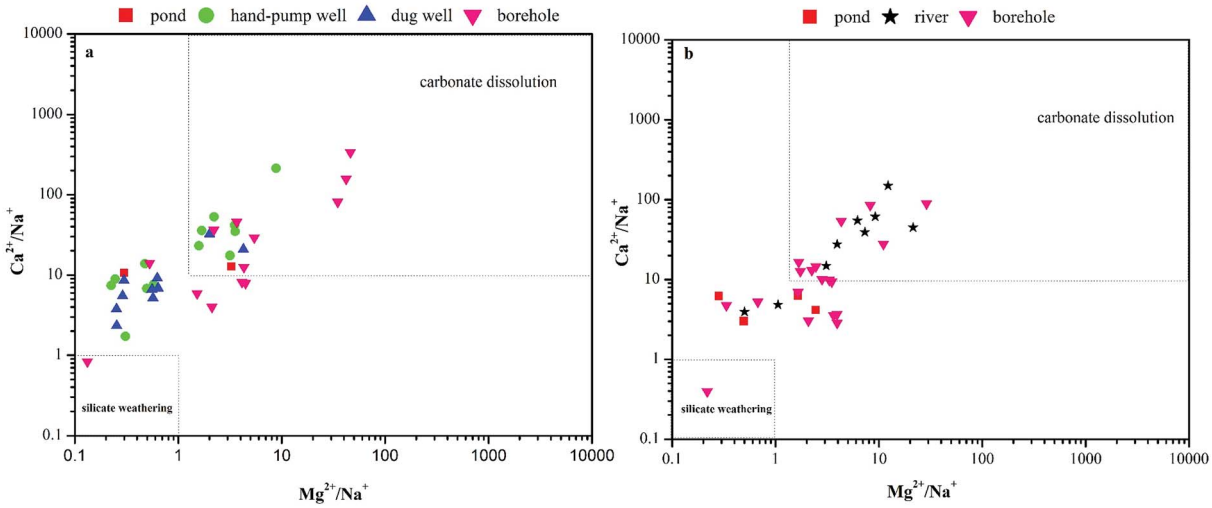

Fig. 9 Bivariate mixing diagram of Na^+ -normalized Mg^{2+} *versus* Na^+ -normalized Ca^{2+} (meq L^{-1}).

exchange.[25] Because pronounced silicate weathering was not seen in the studies waters, a bivariate graph of $(Ca^{2+} + Mg^{2+})$–$(SO_4^{2-} + HCO_3^-)$ *versus* $(Na^+ + K^+–Cl^-)$ (Fig. 9a and b) was plotted to clarify the ionic exchange.[20,26] In the graph (Fig. 10a), a slope of approximately −1 would indicate active cation exchange in the aquifer. The dug well and dry season borehole water samples in the observed area had slopes of −0.53 and 0.04 (Fig. 10a), respectively, indicating that cation exchange had no influence on their water chemistry. Meanwhile, the river and rainy season borehole water samples had slopes of −15.8 and −4.1, respectively, indicating that cation exchange had a slight influence on the water chemistry. Finally, hand-pump well water had a slope of −0.94 (approximately −1), indicating that cation exchange had a substantial influence on the chemistry of hand-pump well water during the dry season.

We also examined two indices of base exchange, namely the chloro-alkaline indices (CAI-1 and CAI-2),[27] to evaluate ion exchange between Na^+ and K^+ in groundwater with Ca^{2+} and Mg^{2+} in the aquifer material.

$$\text{CAI-1} = Cl^- - [(Na^+ + K^+)/Cl^-] \quad (1)$$

$$\text{CAI-2} = Cl^- - [(Na^+ + K^+)/SO_4^{2-}] + HCO_3^- + CO_3^- + NO_3^- \quad (2)$$

The CAI-1 values were negative in most of the water samples (Fig. 11a and b), especially in the pond and borehole water samples during the dry season and all samples during the rainy season. By contrast, the CAI-2 values were positive in the pond and borehole water samples and most of the river, hand-pump well, and dug well water samples. This indicated that Mg^{2+} and Ca^{2+} in groundwater samples are exchanged with Na^+ and K^+ in the aquifer material, and that silicate dissolution or cation exchange may have caused the depletion of some cations in the groundwater samples.

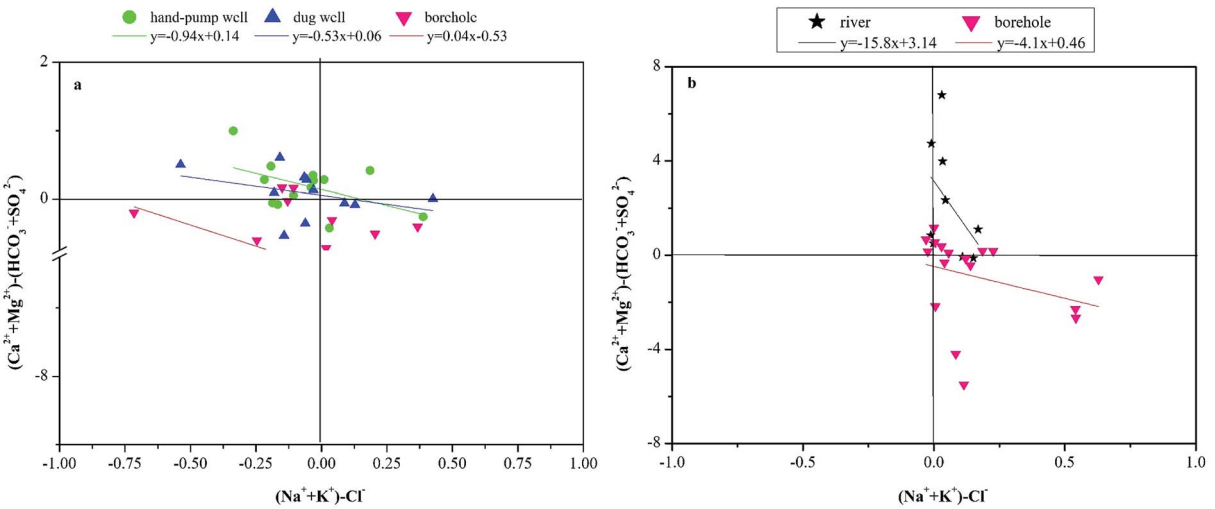

Fig. 10 Bivariate plot of $(Ca^{2+} + Mg^{2+})$–$(HCO_3^- + SO_4^{2-})$ against $(Na^+ + K^+)$–Cl^- (meq L^{-1}).

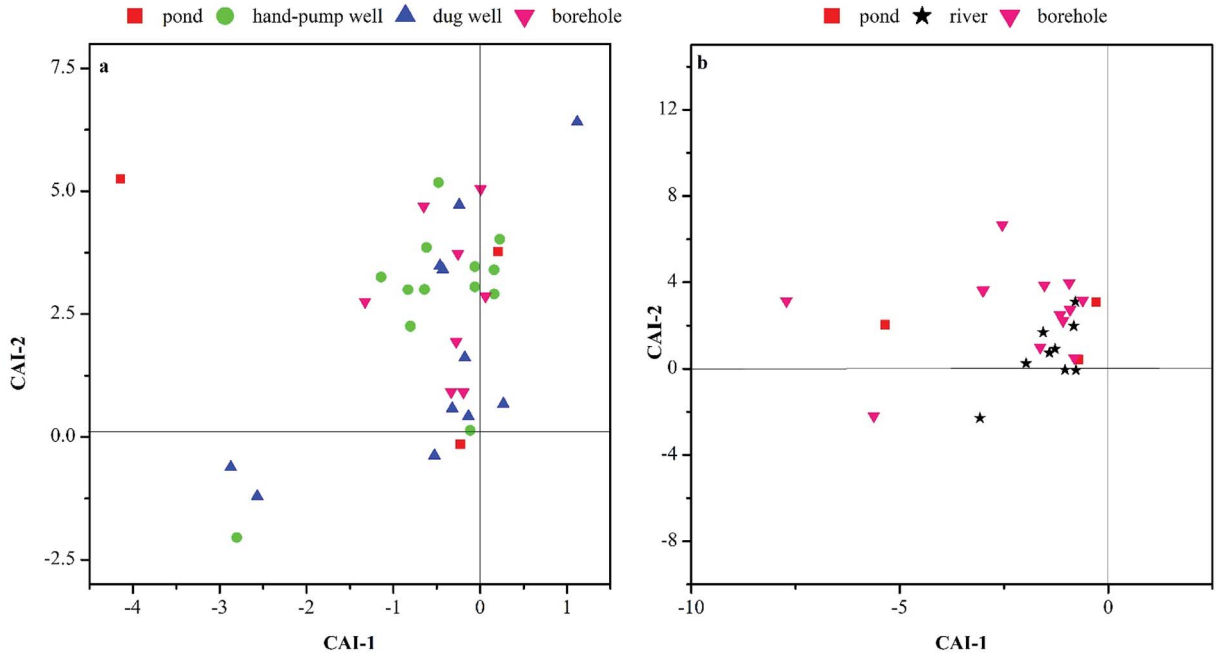

Fig. 11 Plots of CAI-1 *versus* CAI-2.

Ion exchange processes are closely related to groundwater residence time and hydrological conditions.[28] Therefore, the ion exchange in deep water samples was closely related to the residence time according to the aquifer depth. Meanwhile, the shallow groundwater samples were located in a densely populated area. As a consequence of anthropogenic influences, the shallow groundwater samples had higher N, K^+, and Cl^- contents. Generally, groundwater residence time and anthropogenic influences are the main causes of ion exchange in groundwater chemistry.

3.4 Probable sources of potential contaminants

The water samples obtained in the study area were analyzed for heavy metals such as Cr, Mn, Ni, Cu, Zn, As, Cd, and Pb, and the results are shown in Table 2. Mn and Zn were found in relatively high concentrations. The Mn concentrations in ponds, shallow groundwater, and deep groundwater were 0.00–31.4, 0.00–1,871, and 4.94–521 μg L^{-1}, respectively. The Zn concentrations in the surface, shallow, and deep water were 1.32–7.76, 0.00–470, and 0.00–477 μg L^{-1}, respectively. Among the 40 tested water samples, none had heavy metal concentrations exceeding the World Health Organization guidelines[29] or Standards for Drinking Water Quality in China (GB5749-2006).

We performed a principal component analysis (PCA) based on an eigenanalysis of the correlation matrix to identify associations among variables, and indicate the participation of the individual chemical parameters in several influence factors, which is a common phenomenon in hydrochemistry.[30] Only parameters with correlation coefficients exceeding 0.50 were considered. Table 3 presents the correlation matrix of eight heavy metals (Cu and Ni, $r = 0.70$**; Cr and Zn; $r = 0.55$**; As and Zn, $r = 0.51$**; Cd and Cr, $r = 0.60$**; Cd and Zn, $r = 0.94$**; Pb and Cr, $r = 0.56$**; Pb and Zn, $r = 0.71$**; Pb and Cd, $r = 0.86$**). One interpretation of these observations is that, in groundwater, these trace elements had similar hydrochemical

Table 2 Descriptive statistical evaluation of heavy metals in observed waters[a]

	Pond water ($n = 3$)			Shallow groundwater ($n = 24$)			Deep groundwater ($n = 13$)		
μg L^{-1}	Range	Mean	SD	Range	Mean	SD	Range	Mean	SD
Cr	0.02–0.07	0.05	0.02	0.00–0.53	0.08	0.13	0.00–0.51	0.07	0.14
Mn	0.00–31.4	10.60	18.0	0.00–1871	88.9	380	4.94–521	124	161
Ni	0.16–0.59	0.32	0.24	0.00–1.33	0.40	0.33	0.11–4.64	0.32	1.25
Cu	0.20–0.35	0.28	0.07	0.00–1.40	0.34	0.28	0.00–2.65	0.24	0.72
Zn	1.32–7.76	3.58	3.63	0.00–470	32.2	98.7	0.00–477	34.5	132
As	0.00–7.57	3.29	3.88	0.00–1.44	0.35	0.37	0.00–0.65	1.97	0.22
Cd	0.00	0.00	0.00	0.00–0.49	0.03	0.11	0.00–0.81	0.03	0.22
Pb	0.00–0.04	0.01	0.02	0.00–26.0	0.03	0.06	0.00–0.80	0.03	0.22

[a] Shallow groundwater: hand pump well + dug well.

Table 3 Pearson correlation coefficients for the 14 trace elements

	Cr	Mn	Ni	Cu	Zn	As	Cd	Pb
Cr	1.00	−0.16	0.04	0.09	**0.55**[b]	0.29	**0.60**[b]	**0.56**[b]
Mn		1.00	0.15	−0.08	−0.09	−0.25	−0.07	−0.11
Ni			1.00	**0.70**[b]	0.10	0.10	0.14	0.27
Cu				1.00	0.09	0.21	0.12	**0.36**[a]
Zn					1.00	**0.51**[b]	**0.94**[b]	**0.71**[b]
As						1.00	**0.37**[a]	0.25
Cd							1.00	**0.86**[b]
Pb								1.00

[a] Correlation is significant at the 0.05 level. [b] Correlation is significant at the 0.01 level.

characteristics. Trace elements such as Cr and As typically occur as soluble oxyanions in oxidizing waters. Mn is highly soluble in low-pH (reducing) waters. Meanwhile, the redox-sensitive element As is relatively more soluble in oxidized groundwater, where it exists as the oxyanions AsO_4^{2-} and H_2AsO^{4-}. However, in reducing waters, As is readily incorporated in insoluble minerals.

Multivariate statistical methods have been applied widely to investigate environmental phenomena[31] and reduce the dimensionality of data, to allow extraction of information for water quality assessments and surface water management.[32] Among these methods, PCA is often used to simplify large, complex datasets and identify correlated variables, to reduce the number of variables explaining the total variance of the data.[33] In this study, PCA was applied to a dataset containing almost 814 values (22 parameters at 37 sampling sites) to compare the compositional patterns among the examined water systems and identify interrelated factors.

Seven principal components (PCs) had eigenvalues >1, accounting for almost 81.0% of the total variance in the dataset (Table 4). PCs 1–3 explained 19.3%, 17.1%, and 14.4% of the total variance, respectively, accounting for the majority of the variance in the original dataset. PCs 4–7 were less important, and each of these four components explained similar amounts of variance (6.10–10.6%).

PC 1 was significantly correlated with SO_4^{2-}, Fe, and Sr^{2+} concentrations, as well as EC. In the water samples, SO_4^{2-} was mainly derived from the dissolution of gypsum and anhydrite. Meanwhile, the source of Sr might be the dissolution of carbonate rocks or Sr-bearing clay materials.[34] Finally, highly positive loadings for Fe^{2+} may indicate similar geochemical behaviors of these parameters. Therefore, these elements could originate from the dissolution of Fe-oxides and oxidation of sulfide minerals.

PC 2 was correlated with Cr, Zn, Cd, and Pb ion concentrations. Studies have reported that groundwater contamination by heavy metals (*e.g.*, Cd, Cr, Zn, Pb, and Cu) due to agricultural activities is increasing. Cu and Cd are largely related to agronomic practices.[35,36] For example, Cd mainly originates from pesticide application, while fungicides contain large quantities of Cu sulfate.[37] In addition, Zn and Pb originate from industrial and mining activities.[38] Hence, the Cr, Zn, Cd, and Pb ions in

Table 4 Varimax rotated factor matrix for the whole data[a]

	Component						
Variable	PC1	PC2	PC3	PC4	PC5	PC6	PC7
EC	**0.78**	−0.01	0.29	−0.12	−0.04	0.47	0.12
pH	0.28	0.13	−0.24	0.31	−0.41	0.21	0.07
SO_4^{2-}	**0.95**	−0.07	0.09	−0.06	0.07	0.01	−0.01
NO_3^-	−0.09	−0.06	**0.71**	−0.21	0.05	0.40	0.13
Cl^-	0.14	−0.04	**0.87**	−0.08	0.04	0.09	0.02
PO_4^{3-}	0.06	0.11	−0.05	−0.00	−0.17	**0.90**	−0.01
K^+	−0.10	−0.10	**0.79**	0.05	−0.10	−0.05	0.00
Na^+	0.34	−0.04	**0.85**	0.04	0.078	−0.09	0.04
Cr	−0.06	**0.68**	−0.20	0.02	−0.06	0.15	**0.55**
Mn	0.20	−0.07	−0.06	0.06	**0.95**	−0.11	−0.06
Fe	**0.95**	0.08	−0.04	0.03	0.01	−0.14	−0.05
Co	−0.06	0.01	−0.00	0.02	**0.98**	−0.08	−0.00
Ni	−0.03	0.02	−0.08	**0.90**	0.17	0.09	0.01
Cu	−0.12	0.12	0.25	**0.84**	−0.07	−0.04	−0.03
Zn	0.00	**0.91**	−0.02	0.01	0.00	0.23	−0.06
As	−0.11	0.37	0.25	0.11	−0.11	**0.63**	0.01
Se	−0.06	−0.02	0.18	−0.11	−0.08	−0.00	**0.90**
Sr^{2+}	**0.96**	−0.06	−0.10	0.00	0.01	−0.05	−0.05
Mo	0.05	0.21	−0.23	**0.72**	−0.09	−0.04	−0.17
Cd	0.02	**0.96**	−0.11	0.07	−0.01	0.11	−0.05
Ba^{2+}	−0.14	0.37	0.41	0.11	−0.07	0.07	−0.39
Pb	−0.01	**0.86**	−0.03	0.32	−0.07	−0.07	−0.01
% Total variance	19.3	17.1	14.4	10.6	9.80	8.20	6.10
% Cumulative variance	19.3	36.4	50.8	61.3	70.1	75.6	81.0

[a] Significant factor loadings are bold faced.

the water samples in this study were probably derived from a combination of agricultural, mining, and industrial activities.

PC 3 was correlated with NO_3^-, Cl^-, K^+, and Na^+ concentrations. As mentioned by Busico *et al.*,[39] NO_3^-, Cl^-, K^+, and Na^+ can be produced *via* agricultural fertilizer use in rural and suburban areas, as well as from livestock manure and sewer leakages.[40] Therefore, NO_3^-, Cl^-, K^+, and Na^+ were likely the result of agricultural fertilizer inputs, livestock manure, or sewage.

PCs 4–7 explained about 30.2% of the total variance; however, more detailed information is still needed to explore the sources of the ions of these components.

4. Conclusions

We used descriptive statistics, Piper trilinear diagrams, major ion ratios, and PCA to identify the predominant hydrochemical processes and characterize potential contaminants of groundwater in Qingyuan, China. Several conclusions were obtained from the results, as summarized below.

(1) Groundwater in the karst aquifer in Qingyuan is dominated by two main water types, Ca–HCO_3 and Ca–SO_4, controlled mainly by the dissolution of evaporite minerals (*e.g.*, calcite, gypsum, and/or anhydrite) and ion exchange processes.

(2) Na^+ and K^+ concentrations were decreased, while Mg^{2+} was increased in shallow and deep groundwater samples. Overall, shallow groundwater was more vulnerable to pollution than deep groundwater. In addition, the Mg^{2+}/Ca^{2+} ratio was increased in deep groundwater samples because of its relatively long residence time.

(3) Potential contaminants in the karst groundwater were identified by PCA, including NO_3^-, Cl^-, K^+, and Na^+ from agricultural fertilizers, livestock manure, and sewer leakages, as well as Cr, Zn, Cd, and Pb ions, likely from a combination of agricultural, mining, and industrial activities.

Conflicts of interest

There are no conflicts to declare.

Acknowledgements

This work was Supported by the National Natural Science Foundation of China (41701585, 41771027 and 41611140112), the Fundamental Research Fund for the Central Universities of China (17lgpy40), and the Natural Science Foundation of Guangdong, China (2017A030310309), Provincial Special Fund for Economic Development (Marine Economic Development) (GDME2018E004), and the Scientific and Technological Innovation Project of the Water Sciences Department of Guangdong Province (2018-2021) and 1616F G@GPS INQUA.

References

1 X. D. Li, C. Q. Liu, M. Harue, S. L. Li and X. L. Liu, The use of environmental isotopic (C, Sr, S) and hydrochemical tracers to characterize anthropogenic effects on karst groundwater quality: a case study of the Shuicheng Basin, SW China, *Appl. Geochem.*, 2010, **25**(12), 1924–1936.

2 N. Goldscheider and N. Goldscheider, Karst groundwater vulnerability mapping: application of a new method in the Swabian Alb, Germany, *Hydrogeol. J.*, 2005, **13**(4), 555–564.

3 D. K. S. Y. Klaas, M. A. Imteaz, A. Arulrajah, D. K. S. Y. Klaas, M. A. Imteaz and A. Arulrajah, Development of groundwater vulnerability zones in a data-scarce eogenetic karst area using Head-Guided Zonation and particle-tracking simulation methods, *Water Res.*, 2017, **122**, 17–26.

4 Q. Yang, L. Wang, H. Ma, K. Yu and J. D. MartãN, Hydrochemical characterization and pollution sources identification of groundwater in Salawusu aquifer system of Ordos Basin, China, *Environ. Pollut.*, 2016, **216**, 340–349.

5 M. Karroum, M. Elgettafi, A. Elmandour, C. Wilske, M. Himi and A. Casas, Geochemical processes controlling groundwater quality under semi arid environment: a case study in central Morocco, *Sci. Total Environ.*, 2017, **609**, 1140.

6 J. Xiao, Z. Jin and J. Wang, Geochemistry of trace elements and water quality assessment of natural water within the Tarim River Basin in the extreme arid region, NW China, *J. Geochem. Explor.*, 2014, **136**(1), 118–126.

7 S. Armengol, M. Manzano, S. A. Bea and S. Martínez, Identifying and quantifying geochemical and mixing processes in the Matanza-Riachuelo Aquifer System, Argentina, *Sci. Total Environ.*, 2017, **599-600**, 1417.

8 P. W. Swarzenski, C. D. Reich, R. M. Spechler, J. L. Kindinger and W. S. Moore, Using multiple geochemical tracers to characterize the hydrogeology of the submarine spring off Crescent Beach, Florida, *Chem. Geol.*, 2001, **179**(1), 187–202.

9 H. C. LI Yan, Characteristics and mechanism of manufacturing industry shift in the Pearl River Delta during 1998-2009, *Progress in Geography*, 2013, **32**(5), 777–787.

10 H. Ji and Y. Jiang, Carbon flux and C, S isotopic characteristics of river waters from a karstic and a granitic terrain in the Yangtze River system, *J Asian Earth Sci.*, 2012, **57**(3), 38–53.

11 P. Négrel, C. J. Allègre, B. Dupré and E. Lewin, Erosion sources determined by inversion of major and trace element ratios and strontium isotopic ratios in river water: The Congo Basin case, *Earth Planet. Sci. Lett.*, 1993, **120**(1–2), 59–76.

12 X. F. Huang, X. A. Li, L. Y. He, N. Feng, M. Hu, Y. W. Niu and L. W. Zeng, 5-Year study of rainwater chemistry in a coastal mega-city in South China, *Atmos. Res.*, 2010, **97**(1), 185–193.

13 C. Soulsby, M. Chen, R. C. Ferrier, R. C. Helliwell, A. Jenkins and R. Harriman, Hydrogeochemistry of shallow groundwater in an upland Scottish catchment, *Hydrol. Processes*, 2015, **12**(7), 1111–1127.

14 Ž. Brkić, M. Briški and T. Marković, Use of hydrochemistry and isotopes for improving the knowledge of groundwater flow in a semiconfined aquifer system of the Eastern Slavonia (Croatia), *Catena*, 2016, **142**, 153–165.

15 H. Jiráková, F. Huneau, Z. Hrkal, H. Celle-Jeanton and P. L. Coustumer, Carbon isotopes to constrain the origin and circulation pattern of groundwater in the north-

western part of the Bohemian Cretaceous Basin (Czech Republic), *Appl. Geochem.*, 2010, **25**(8), 1265–1279.

16 S. Jakóbczyk-Karpierz, S. Sitek, R. Jakobsen and A. Kowalczyk, Geochemical and isotopic study to determine sources and processes affecting nitrate and sulphate in groundwater influenced by intensive human activity - carbonate aquifer Gliwice (Southern Poland), *Appl. Geochem.*, 2016, **76**, 168–181.

17 H. Celle-Jeanton, C. Emblanch, J. Mudry and A. Charmoille, Contribution of time tracers (Mg^{2+}, TOC, $\delta^{13}C_{TDIC}$, NO_3^-) to understand the role of the unsaturated zone: A case study—Karst aquifers in the Doubs valley, eastern France, *Geophys. Res. Lett.*, 2016, **30**(6), 7027.

18 K. A. R. Kpegli, A. Alassane, R. Trabelsi, K. Zouari, M. Boukari, D. Mama, F. L. Dovonon, Y. V. Yoxi and L. E. Toro-Espitia, Geochemical processes in Kandi Basin, Benin, West Africa: A combined hydrochemistry and stable isotopes approach, *Quat. Int.*, 2015, **369**, 99–109.

19 M. Meybeck, Global chemical weathering of surficial rocks estimated from river dissolved loads, *Am. J. Sci.*, 1987, **287**(5), 401–428.

20 I. Farid, R. Trabelsi, K. Zouari and R. Beji, Geochemical and isotopic study of surface and groundwaters in Ain Bou Mourra basin, central Tunisia, *Quat. Int.*, 2013, **303**(4), 210–227.

21 J. He, Y. An and F. Zhang, Geochemical characteristics and fluoride distribution in the groundwater of the Zhangye Basin in Northwestern China, *J. Geochem. Explor.*, 2013, **135**(6), 22–30.

22 Q. Yang, L. Wang, H. Ma, K. Yu and J. D. Martín, Identification of the hydrogeochemical processes and assessment of groundwater quality using classic integrated geochemical methods in the Southeastern part of Ordos basin, China, *Environ. Pollut.*, 2016, **218**, 879–888.

23 F. Marcantonio, Principles and Applications of Geochemistry, *Trans., Am. Geophys. Union*, 2013, **79**(30), 356.

24 W. Edmunds, A. Guendouz, A. Mamou, A. Moulla, P. Shand and K. Zouari, Groundwater evolution in the Continental Intercalaire aquifer of southern Algeria and Tunisia: trace element and isotopic indicators, *Appl. Geochem.*, 2003, **18**(6), 805–822.

25 J. Ma, Z. Ding, W. M. Edmunds, J. B. Gates and T. Huang, Limits to recharge of groundwater from Tibetan plateau to the Gobi desert, implications for water management in the mountain front, *J. Hydrol.*, 2009, **364**(1), 128–141.

26 A. B. Moussa, H. Mzali, K. Zouari and H. Hezzi, Hydrochemical and isotopic assessment of groundwater quality in the Quaternary shallow aquifer, Tazoghrane region, north-eastern Tunisia, *Quat. Int.*, 2014, **338**(4), 51–58.

27 H. Schoeller, Hydrodynamique dans le karst, *Chron. Hydrogeol.*, 1967, **10**, 7–21.

28 H. Guo and Y. Wang, Hydrogeochemical processes in shallow quaternary aquifers from the northern part of the Datong Basin, China, *Appl. Geochem.*, 2004, **19**(1), 19–27.

29 F. Edition, *Guidelines for drinking-water quality*, WHO chronicle, 2011, vol. 38, pp. 104–108.

30 K. Chen, J. J. Jiao and J. Huang, Multivariate statistical evaluation of trace elements in groundwater in a coastal area in Shenzhen, China, *Environ. Pollut.*, 2007, **147**(3), 771–780.

31 K. Anazawa and H. Ohmori, The hydrochemistry of surface waters in andesitic volcanic area, Norikura volcano, central Japan, *Chemosphere*, 2005, **59**(5), 605–615.

32 V. Simeonov, J. Stratis, C. Samara, G. Zachariadis, D. Voutsa, A. Anthemidis, M. Sofoniou and T. Kouimtzis, Assessment of the surface water quality in Northern Greece, *Water Res.*, 2003, **37**(17), 4119–4124.

33 R. P. Hooper, Diagnostic tools for mixing models of stream water chemistry, *Water Resour. Res.*, 2003, **39**(3), 249–256.

34 M. Zieliński, J. Dopieralska, Z. Belka, A. Walczak, M. Siepak, M. Jakubowicz, M. Zieliński, J. Dopieralska, Z. Belka, *et al.*, The strontium isotope budget of the Warta River (Poland): between silicate and carbonate weathering, and anthropogenic pressure, *Appl. Geochem.*, 2017, **81**, 1–11.

35 J. Nouri, A. H. Mahvi, G. R. Jahed and A. A. Babaei, Regional distribution pattern of groundwater heavy metals resulting from agricultural activities, *Environ. Geol.*, 2008, **55**(6), 1337–1343.

36 P. Wongsasuluk, S. Chotpantarat, W. Siriwong and M. Robson, Heavy metal contamination and human health risk assessment in drinking water from shallow groundwater wells in an agricultural area in Ubon Ratchathani province, Thailand, *Environ. Geochem. Health*, 2014, **36**(1), 169–182.

37 L. Gao, Z. Wang, J. Shan, J. Chen, C. Tang and M. Yi, Aquatic environmental changes and anthropogenic activities reflected by the sedimentary records of the Shima River, Southern China, *Environ. Pollut.*, 2017, **224**, 70–81.

38 A. Bartkowiak, J. Lemanowicz and B. Breza-Boruta, Evaluation of the content of Zn, Cu, Ni and Pb as well as the enzymatic activity of forest soils exposed to the effect of road traffic pollution, *Environ. Sci. Pollut. Res.*, 2017, **24**(30), 23893–23902.

39 G. Busico, E. Cuoco, N. Kazakis, N. Colombani, M. Mastrocicco, D. Tedesco and K. Voudouris, Multivariate statistical analysis to characterize/discriminate between anthropogenic and geogenic trace elements occurrence in the Campania Plain, Southern Italy, *Environ. Pollut.*, 2018, **234**, 260–269.

40 E. Cuoco, N. Colombani, Ograve, T. H. Darrah, M. Mastrocicco, D. Tedesco, E. Cuoco, N. Colombani, T. H. Darrah, *et al.*, Geolithological and anthropogenic controls on the hydrochemistry of the Volturno river (Southern Italy), *Hydrol. Processes*, 2017, **31**, 627–638.